



Improved Carroll's hyperelastic model considering compressibility and its finite element implementation

Stephen Kirwa Melly¹ · Liwu Liu¹ · Yanju Liu¹ · Jinsong Leng²

Received: 9 December 2020 / Accepted: 11 January 2021 / Published online: 11 March 2021

© The Chinese Society of Theoretical and Applied Mechanics and Springer-Verlag GmbH Germany, part of Springer Nature 2021

Abstract

In engineering component design, material models are increasingly used in finite element simulations for an expeditious and less costly analysis of the design prototypes. As such, researchers strive to formulate models that are less complex, robust, and accurate. In the realm of hyperelastic materials, phenomenological-based Carroll's model is highly promising due to its simplicity and accuracy. This work proposes its further improvement by modifying the strain energy density function to comply with the restriction that it should vanish at reference configuration and adding a compressible term to capture the practical behavior of elastomeric materials and to avoid numerical problems during finite element implementation. The model constants for both the original and the modified versions were obtained by fitting their respective expressions to the classical Treloar's experimental data using the Levenberg–Marquardt algorithm. The modified model was implemented using Abaqus CAE 2016 via a vectorized user material (VUMAT) subroutine. Comparisons of the model predictions with Treloar's experimental data demonstrated the superiority of the modified version particularly in the equibiaxial loading mode. Moreover, the simulated and the experimentally observed behavior agreed to a great accuracy thus making the modified model suitable for simulating the loading response of components fabricated of elastomeric materials.

Keywords Elastomers · Rubber-like · Strain energy function · Finite deformation

1 Introduction

The extensive utilization of elastomeric materials particularly in fabricating engineering components for aerospace and automotive industries has subjected them to huge research efforts in the last several decades. Understanding the mechanical behavior of these materials when subjected to various kinds of loads is crucial for the optimum design of components and predicting the response in practical applications. Unlike linear elastic materials where Hook's law suffices in predicting mechanical response provided that

the elastic constants are known, the nonlinear stress–strain relationship of the elastomeric materials makes the Hook's law inadequate since definitive elastic constants especially at large deformations can't be obtained. Consequently, the theory of nonlinear elasticity was pioneered by Mooney [1] in the early 1940s. In this theory, also known as hyperelasticity theory, the stress–strain relationship is derived from a function known as strain energy density (Ψ) that is specific to the hyperelastic materials and is dependent on the deformation gradient [2, 3]. Formulation of the strain energy density function expression assumes that the hyperelastic material is isotropic, homogenous, strain-rate independent, free of hysteresis, and incompressible [4]. There are mathematical restrictions on strain energy density functions and have been listed in several texts [5, 6] some of which include; must be non-negative for all deformations, must vanish in the reference configuration, and must be invariant under a coordinate transformation.

Formulation of the strain energy density function and ultimately the constitutive relation takes either of the two approaches; micro-mechanical or phenomenological. The former involves the utilization of statistical mechanics

Executive Editor: Shao-Xing Qu

✉ Liwu Liu
liuliuw_006@163.com

✉ Jinsong Leng
lengjs@hit.edu.cn

¹ Department of Astronautical Science and Mechanics, Harbin Institute of Technology (HIT), Harbin 150001, China

² Center for Composite Materials and Structures, Harbin Institute of Technology (HIT), Harbin 150080, China

techniques to describe the behavior of long-chain polymeric networks at the microscopic level of the material. Examples of such models include the eight-chain [7], Flory-Erman [8], and the extended-tube model [9]. The latter involves fitting of mathematical equations to the experimental data of the material and generally results in polynomial formulations that are based on the strain invariants or principal stretches [5]. There are dozens of phenomenological models in the literature and some of the well-known examples include Neo-Hookean [10], Yeoh [11], Mooney-Rivlin [1, 12], and Horgan-Saccomandi [13]. Hybrid models (those that combine both the phenomenological and micro-mechanical approaches) also exist in Ref. [14]. Readers interested in a better understanding of these models may read some of the comprehensive reviews such as those of Boyce and Arruda [15], Carroll [16], Beda [17], and the dissertation work of Badienia [18].

The classical experimental data by Treloar [19] has been the main reference in both the formulation and the determination of the accuracy of new models. It contains the stress-stretch data for different modes of loading including uniaxial tension, equibiaxial tension, and pure shear. A model that can accurately reproduce the experimental data in all of the three loading modes and requires a single set of few material parameters is considered the best. However, the majority of the existing models can be accurate in one loading mode such as uniaxial tension but fail in the other modes. Additionally, they may require a different set of material parameters for each of the loading modes. These challenges motivate researchers to formulate new models or improve the existing ones. Kaoye et al. [20] improved the Gent model to better predict the equibiaxial deformation. Miroshnychenko and Green [21] developed a model that was an improvement of the eight-chain model [7]. The new model could outperform the latter and other well-known models such as the Ogden model in replicating Treloar's experimental data. Noting that the majority of the hyperelastic models neglect the temperature-dependent behavior of elastomeric materials, Fu et al. [22] modified the eight-chain model to achieve a constitutive relation that considers the temperature effects. In addition to the improvement of existing models, various research groups focus on the development of new models aimed at better prediction performance. Yaya and Bechir [23] followed the phenomenological approach to develop a four-parameter model that performed as good as the Ogden six-parameter model. Khajehsaeid et al. [24] developed a three-parameter model whose parameters are independent of the deformation mode. This is advantageous in that a single experimental test is required to calibrate the model. Whilst the majority of the strain energy density functions are based on the invariants of the Cauchy-Green deformation tensor,

Zhao et al. [25] formulated a new model basing on the invariants of the Seth strain tensor. The model performed better in comparison to the Yeoh model and could predict behavior in a wide range of deformations. Recently, Külcü [26] proposed a new strain energy density expression based on the strain invariants with only two material parameters that could work in different loading modes. Amongst the most interesting and recent models is the one by Carroll [27]. Its strain energy density function was formulated based on a phenomenological approach and has three material parameters. It has remarkable accuracy especially in the uniaxial tension and pure shear loading in terms of Treloar's experimental data. By comparing fourteen models, Steinmann et al. [28] found the accuracy of Carroll's model particularly in pure shear loading to be unmatched by any models.

Recognizing the simplicity, accuracy, and potential of Carroll's model to be utilized for predicting the mechanical response of elastomeric materials under various loading conditions, this work aims to improve the said model for even better performance and applicability. The choice of Carroll's model for improvement is not arbitrary but based on its relative advantages when compared to other hyperelastic models with good predictions in uniaxial tension and pure shear loading. It requires only three material constants yet its performance in uniaxial tension matches that of the extended-tube model [9] and Ogden [29] which require five and seven material constants respectively. Due to its phenomenological nature, the material constants have no physical meaning and, therefore, the knowledge on the material microstructure is not necessary to obtain the parameters but rather by fitting the experimental data to the model equation using nonlinear least-squares methods. Importantly, it requires a single pair of model constants to predict the behavior in multi-axial loading and the model equation can be implemented in a finite element program. However, a closer look at its strain energy density expression shows that it doesn't satisfy one of the mathematical restrictions (it should vanish in the reference configuration). This affects the accuracy of the parameters and ultimately that of the predictions of the model. Again, the formulation assumes that the material is incompressible (just like the majority of the models). Whilst this assumption simplifies the expressions and provides good approximations, numerical problems such as element locking arise during finite element implementation [30]. Therefore, to enable complex problem analysis via finite element simulations, compressibility must be taken into consideration. The objectives of this work include; modify the strain energy density expression according to the mathematical restriction mentioned, incorporate a compressibility term in the expression, and implement the model in a finite element code.

2 Strain energy density

2.1 Formulation

Since the strain energy density of a phenomenological model is a function of the invariants of the strain tensors or the principal stretches, knowledge of continuum mechanics is essential. A body undergoing finite deformation has \mathbf{x} and \mathbf{X} vectors represent the material points in the deformed and the undeformed configurations respectively. The deformation gradient relates these two configurations and is given by the partial derivative of each component of the deformed vector with respect to each component of the undeformed vector, $\mathbf{F} = \frac{\partial \mathbf{x}}{\partial \mathbf{X}}$. According to the polar decomposition theorem, \mathbf{F} can be multiplicatively decomposed into a proper orthogonal tensor (pure rotation tensor) and a symmetric positive-definite tensor (pure stretch tensor) [31]. The left and the right decompositions of \mathbf{F} are given in Eq. (1)

$$\mathbf{F} = \mathbf{V} \cdot \mathbf{R} = \mathbf{R} \cdot \mathbf{U}, \tag{1}$$

where \mathbf{V} and \mathbf{U} are the left and right Cauchy stretch tensors respectively whereas \mathbf{R} is the orthogonal rotation tensor. The left and the right Cauchy-Green deformation tensors are given by $\mathbf{B} = \mathbf{F} \cdot \mathbf{F}^T$ and $\mathbf{C} = \mathbf{F}^T \cdot \mathbf{F}$ respectively. The relationship between deformation and stretch tensors can be found by applying Eq. (1) to expressions for \mathbf{B} and \mathbf{C} as shown in Eq. (2)

$$\begin{aligned} \mathbf{B} &= \mathbf{F} \cdot \mathbf{F}^T = (\mathbf{V} \cdot \mathbf{R}) \cdot (\mathbf{V} \cdot \mathbf{R})^T = \mathbf{V} \cdot \mathbf{R} \cdot \mathbf{R}^T \cdot \mathbf{V}^T = \mathbf{V}^2, \\ \mathbf{C} &= \mathbf{F}^T \cdot \mathbf{F} = (\mathbf{R} \cdot \mathbf{U})^T \cdot (\mathbf{R} \cdot \mathbf{U}) = \mathbf{U}^T \cdot \mathbf{R}^T \cdot \mathbf{R} \cdot \mathbf{U} = \mathbf{U}^2. \end{aligned} \tag{2}$$

From Eq. (2), it is worth noting that $\mathbf{R}^T \cdot \mathbf{R} = \mathbf{R} \cdot \mathbf{R}^T = \mathbf{I}$. Both \mathbf{V} and \mathbf{U} have identical eigenvalues which are classically denoted as λ_1, λ_2 and λ_3 . These eigenvalues are the principal stretches of deformation.

The invariants of \mathbf{C} , which are the same as those of \mathbf{B} , are obtained as shown in Eq. (3)

$$\begin{aligned} I_1 &= \text{tr} \mathbf{C} = \lambda_1^2 + \lambda_2^2 + \lambda_3^2, \\ I_2 &= \frac{1}{2} [(\text{tr} \mathbf{C})^2 - \text{tr}(\mathbf{C}^2)] = \lambda_1^2 \lambda_2^2 + \lambda_2^2 \lambda_3^2 + \lambda_3^2 \lambda_1^2, \\ I_3 &= \det \mathbf{C} = \lambda_1^2 \lambda_2^2 \lambda_3^2. \end{aligned} \tag{3}$$

The invariant-based phenomenological models have their strain energy density as a function of the invariants of \mathbf{C} given in Eq. (3) and expressed as $\Psi(I_1, I_2, I_3)$. Simplification is achieved when the material is assumed to be incompressible (no volume change during deformation). The ratio of the volume in the deformed to the undeformed configuration (V/V_0) is given by the Jacobian determinant of the deformation gradient, $J = \det \mathbf{F} = \lambda_1 \lambda_2 \lambda_3 = \sqrt{I_3}$. Incompressibility assumption means that $J = I_3 = 1$, thus, making the strain

energy density a function of the first and second invariants $\Psi(I_1, I_2)$. Generally, the inclusion of the second invariant improves the accuracy of the model especially on the biaxial loading and capturing the strain-stiffening with an increase in stretch values [32].

The expression for the Cauchy stress is derived from the strain energy density expression and an elaborate derivation process is presented by Bergström [33]. For an arbitrary loading and assuming incompressibility, the Cauchy stress is obtained as shown in Eq. (4)

$$\sigma = 2 \left(\frac{\partial \Psi}{\partial I_1} + \frac{\partial \Psi}{\partial I_2} I_1 \right) \mathbf{B} - 2 \frac{\partial \Psi}{\partial I_2} \mathbf{B}^2 + p \mathbf{I}, \tag{4}$$

where p is a pressure term due to incompressibility and is determined from the boundary conditions and \mathbf{I} is the identity tensor. On the other hand, the Cauchy stress expression for an arbitrary loading that considers compressibility is given in Eq. (5)

$$\sigma = \frac{2}{J} \left(\frac{\partial \Psi}{\partial I_1} + \frac{\partial \Psi}{\partial I_2} I_1 \right) \mathbf{B} - \frac{2}{J} \frac{\partial \Psi}{\partial I_2} \mathbf{B}^2 + \left(\frac{\partial \Psi}{\partial J} - \frac{2I_1}{3J} \frac{\partial \Psi}{\partial I_1} - \frac{4I_2}{3J} \frac{\partial \Psi}{\partial I_2} \right) \mathbf{I}, \tag{5}$$

The main features of Carroll's model are; has three parameters, depends on both the first and second invariants, and assumes the incompressibility of the material. Full details on its derivation are found in Carroll's original work [27]. Using Treloar's data, the strain energy density function for Carroll's model was developed in three steps as demonstrated in Table 1.

The overall strain energy density function for Carroll's model is finally obtained by summing the individual strain energies of each step resulting in the expression shown in Eq. (6)

$$\Psi(I_1, I_2) = \beta_1 I_1 + \beta_2 I_1^4 + \beta_3 \sqrt{I_2}, \tag{6}$$

where β_1, β_2 and β_3 are the material parameters to be determined by fitting Treloar's data.

As already mentioned, some mathematical restrictions were postulated by influential researchers Ogden [6] and Treloar [10]. One of these restrictions is that the strain energy density must vanish at the reference configuration $\Psi(I_1, I_2, I_3) = 0$. The physical meaning of this particular restriction is that the material has zero stress at the undeformed state. The principal stretches at the undeformed state are given by $\lambda_1 = \lambda_2 = \lambda_3 = 1$. The corresponding values of the invariants are given in Eq. (7)

$$\begin{aligned} I_1 &= \lambda_1^2 + \lambda_2^2 + \lambda_3^2 = 3, \\ I_2 &= \lambda_1^2 \lambda_2^2 + \lambda_2^2 \lambda_3^2 + \lambda_3^2 \lambda_1^2 = 3, \\ I_3 &= \lambda_1^2 \lambda_2^2 \lambda_3^2 = 1. \end{aligned} \tag{7}$$

Table 1 Development of Carroll's strain energy density function

Step	Notes	Strain energy density expression
1	Treloar's uniaxial tension stress-stretch data in the range $1 < \lambda < 4.5$ has its strain energy linearly dependent on I_1 and can be approximated by the Neo-Hookean strain energy density function $\Psi = \beta_1 I_1$. The stress equation for uniaxial tension loading is found to be $\sigma_1^{\text{UT}} = 2\beta_1 \left(\lambda - \frac{1}{\lambda^2} \right)$.	$\Psi = \beta_1 I_1$
2	Taking Treloar's uniaxial tension stress-stretch data as (σ_u, λ_u) , the residual stress (stress that is not accounted for by the stress equation in step 1) can be found by $\sigma_{\text{res}}^{\text{UT}} = \sigma_u - 2\beta_1 \left(\lambda_u - \frac{1}{\lambda_u^2} \right)$. The strain energy density for the residual stress is approximated by the expression $\Psi = \beta_2 I_1^4$ and its corresponding stress equation is $\sigma_2^{\text{UT}} = 8\beta_2 \left(\lambda - \frac{1}{\lambda^2} \right) \left(\lambda^2 + \frac{2}{\lambda} \right)^3$.	$\Psi = \beta_2 I_1^4$
3	Lastly, the residual stress in equibiaxial tension (stress that is not accounted for by both of the stress equations in steps 1 and 2) is modeled. Taking $(\sigma_{\text{eb}}, \lambda_{\text{eb}})$ as Treloar's stress-stretch data in equibiaxial loading, the residual stress is found as $\sigma_{\text{res}}^{\text{EB}} = \sigma_{\text{eb}} - 2 \left(\lambda_{\text{eb}} - \frac{1}{\lambda_{\text{eb}}^2} \right) \left[\beta_1 + 4\beta_2 \left(2\lambda_{\text{eb}}^2 + \frac{1}{\lambda_{\text{eb}}^4} \right)^3 \right]$. The strain energy density function for the residual stress is approximated by the expression $\Psi = \beta_3 \sqrt{I_2}$.	$\Psi = \beta_3 \sqrt{I_2}$

Applying this to Carroll's strain energy density function given in Eq. (6) yields the strain energy of the model at the reference configuration as shown in Eq. (8)

$$\Psi(3, 3) = 3\beta_1 + 81\beta_2 + \beta_3\sqrt{3}, \quad (8)$$

Since $\beta_1 = \beta_2 = \beta_3 \neq 0$, the strain energy of Carroll's model will have a nonzero value at the reference configuration which violates one of the main restrictions. This influences the material parameters and consequently the predictions of the model. For this reason, we propose the modification of Eq. (6) to Eq. (9)

$$\Psi(I_1, I_2) = \beta_1(I_1 - 3) + \beta_2(I_1^4 - 81) + \beta_3(\sqrt{I_2} - \sqrt{3}). \quad (9)$$

It is easy to find that the modified Carroll's strain energy density expression given in Eq. (9) satisfies the postulate that strain energy must be zero at the reference configuration as shown in Eq. (10)

$$\Psi(3, 3) = 0. \quad (10)$$

2.2 Compressibility

Whilst incompressibility is a common assumption in the modeling of elastomeric materials, it is merely an approximation of the material behavior. The realistic behavior involves volume changes and, therefore, compressibility is necessary for more accurate predictions of the model.

For instance, elastomeric materials subjected to hydrostatic compression undergo substantial volume changes which are up to 20% of the initial volume, thus, making incompressible models inaccurate [34]. The incompressibility assumption is advantageous in that it leads to simplified mathematical equations that describe the mechanical behavior of elastomers and give a good approximation [35]. However, numerical problems that lead to non-convergence of the solution arise during the finite element implementation of the incompressible models to simulate complex material deformations [15, 36]. With the increased usage of finite element simulations to understand the behavior of product prototypes, there is a need to develop constitutive models that consider volume changes during deformation.

The first step in accounting for volume changes is to remove the restriction that $I_3 = 1$ and taking the volume ratio $J = \sqrt{I_3}$. The strain energy density is then taken to be composed of two parts (see Eq. (11)); the deviatoric/distortional and the hydrostatic/volumetric parts which are responsible for shape and volume changes respectively

$$\Psi = \Psi_D(I_1^*, I_2^*) + \Psi_H(J), \quad (11)$$

where the subscripts D and H stand for deviatoric and hydrostatic respectively whereas I_1^* and I_2^* are the invariants of the deviatoric left or right Cauchy-Green deformation tensor. From the deviatoric part of the deformation gradient, $\mathbf{F}^* = J^{-(1/3)}\mathbf{F}$, the deviatoric left and right Cauchy-Green deformation tensors are given by $\mathbf{B}^* = \mathbf{F}^*(\mathbf{F}^*)^T = J^{-(2/3)}\mathbf{B}$ and $\mathbf{C}^* = (\mathbf{F}^*)^T\mathbf{F}^* = J^{-(2/3)}\mathbf{C}$ respectively. The deviatoric invariants are then given by the expressions in Eq. (12)

$$\begin{aligned}
 I_1^* &= \text{tr} \mathbf{C}^* = J^{-2/3} I_1, \\
 I_2^* &= \frac{1}{2} \left[(\text{tr} \mathbf{C}^*)^2 - \text{tr}(\mathbf{C}^{*2}) \right] = J^{-4/3} I_2.
 \end{aligned}
 \tag{12}$$

On the other hand, the hydrostatic term is related to the volume ratio and the bulk modulus of the material as shown in Eq. (13)

$$\Psi_H = \frac{K}{2} (J - 1)^2,
 \tag{13}$$

where K is the bulk modulus. Using Eqs. (9), (11)–(13), the modified Carroll's strain energy density function is given by Eq. (14)

$$\begin{aligned}
 \Psi(I_1^*, I_2^*, J) &= \beta_1 (I_1^* - 3) + \beta_2 (I_1^{*4} - 81) \\
 &\quad + \beta_3 \left(\sqrt{I_2^*} - \sqrt{3} \right) + \frac{K}{2} (J - 1)^2.
 \end{aligned}
 \tag{14}$$

2.3 Material parameters

The material parameters in a phenomenological model have no physical meaning and must be determined by fitting the model to experimental data. Treloar [19] presented nominal stress-stretch data for 8% Sulfur vulcanized rubber under three deformation modes; uniaxial tension, equibiaxial tension, and pure shear. Treloar's data has been extremely useful for developing hyperelastic models since it involves large stretch values. The unit of stress in Treloar's data is kg/cm² and was converted to Nm/m² in this work for convenience. The stretch λ was also converted to engineering strain using the relation $\epsilon = \lambda - 1$. Consequently, Treloar's engineering stress–strain data plot for the three modes of loading is shown in Fig. 1a. Since the material parameters are obtained by fitting the strain energy density expression to the strain

energy in the material due to loading, the strain energy/unit volume data must be calculated from the stress–strain data (given area under the stress–strain curve). Since the material parameters for Carroll's model in one loading mode work for all loading modes, only the uniaxial tension data was considered in this work for obtaining the parameters. The Trapezoidal rule was utilized to calculate the area under the stress–strain curve of uniaxial tension loading and the strain energy/unit volume against strain was plotted as shown in Fig. 1b.

Since the relationship between the strain energy and the strain is nonlinear as shown in Fig. 1b, fitting the strain energy density function to the data to get the parameters is a nonlinear least-squares problem. Several numerical algorithms are available for solving nonlinear least-squares problems [37]. The Levenberg–Marquardt algorithm (LMA) [38, 39] is a robust, efficient, and popular method for solving nonlinear least-squares problems. It has been utilized in determining the material parameters for hyperelastic models [40]. In this work, the LMA was implemented in a Python code (see Fig. 2) to find the material parameters for both the original and the modified Carroll's model strain energy density function given in Eqs. (6) and (14) respectively. The coefficient of determination, denoted as R^2 , as shown in Eq. (15) is utilized to determine how well the model with the material parameters predicts the observed experimental behavior

$$R^2 = 1 - \frac{\sum_{i=1}^n (e_i - p_i)^2}{\sum_{i=1}^n (e_i - e_m)^2},
 \tag{15}$$

where n is number of data points, e_i is experimental data at a point i , p_i is prediction data at a point i , and e_m is the mean of the experimental data.

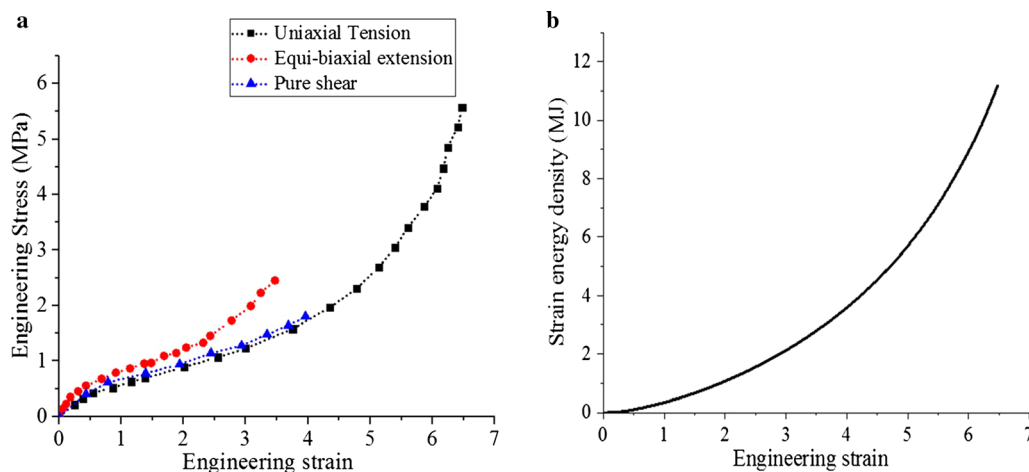


Fig. 1 **a** Stress–strain plots of the Treloar's experimental data for uniaxial tension, equibiaxial tension, and pure shear loading and **b** the calculated strain energy density against engineering strain for uniaxial loading mode

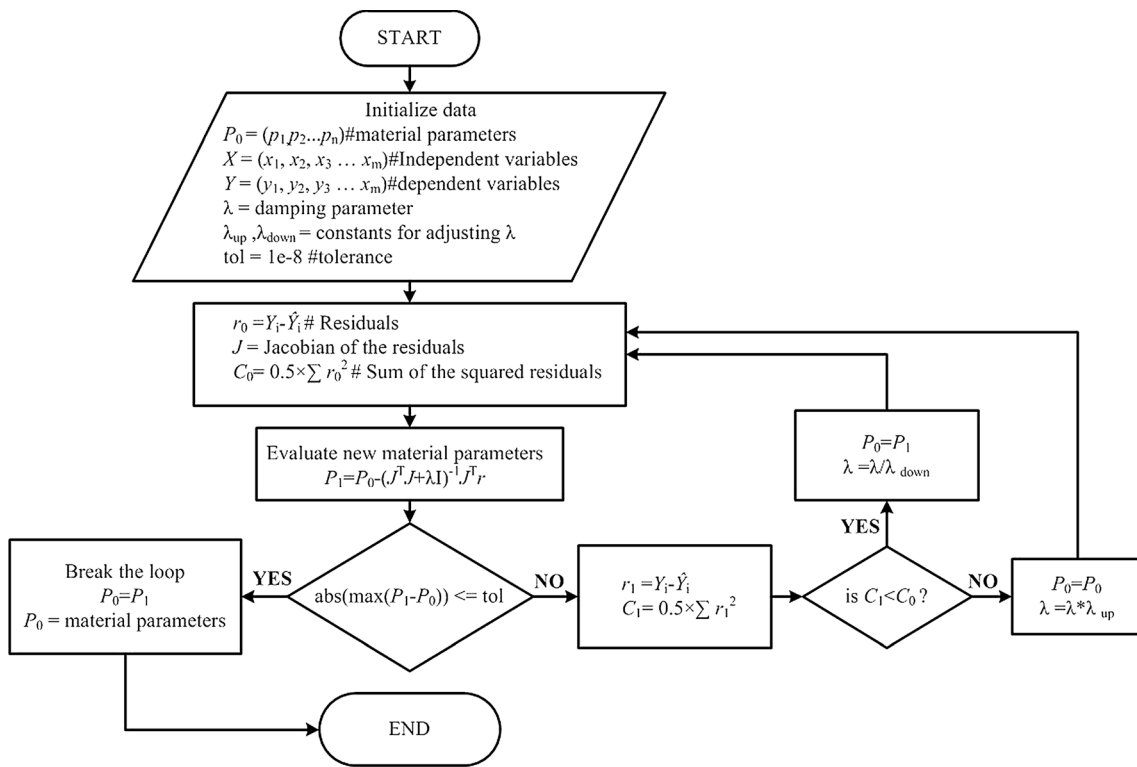


Fig. 2 Flowchart for implementing the Levenberg–Marquardt algorithm

Table 2 Material parameters

Model	Iterations	Parameters			
		$\beta_1(\text{Pa})$	$\beta_2(\text{Pa})$	$\beta_3(\text{Pa})$	$K(\text{Pa})$
Carroll's	4	166,333.95	0.2710	-233,047.21	-
Modified	11	151,093.87	0.3028	68,330.70	5×10^8

The material parameters obtained for both the original and modified Carroll’s models are given in Table 2. The bulk modulus was obtained from the literature. With the parameters, corresponding model predictions according to Eqs. (6) and (14) were obtained and compared with the calculated strain energy density from the experimental uniaxial loading data. As shown in Fig. 3, the predictions were exceptionally accurate (R^2 values very close to unity) such that it can be difficult to differentiate the curves. It can be observed that the original Carroll’s model predictions deviate from the experimental data at zero strains since it records some strain energy (approximately 95,374.20 J).

3 Numerical and finite element (FE) implementation

The ultimate goal of model development is to implement it in FE software to simulate the material response when subjected to various loading conditions. Finite element

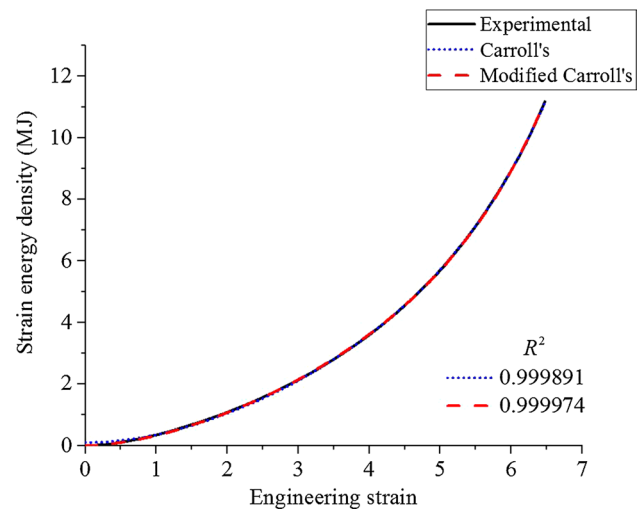


Fig. 3 Comparison of the predicted and the calculated strain energy density for uniaxial tension loading

simulation is nowadays an indispensable part of a product design process as it provides, depending on the accuracy of the model, an accurate approximation of the material response whilst saving on cost and time.

The requirement for both the numerical and FE implementation is the Cauchy stress equation for an arbitrary loading. Given the strain energy density function expressions for the original and modified Carroll's models in Eqs. (6) and (14) respectively, their corresponding Cauchy stress expressions for arbitrary loading are found by applying Eqs. (4) and (5) respectively. The resulting Cauchy stress equations are given in Eqs. (16) and (17) respectively

$$\sigma = 2 \left(\beta_1 + 4\beta_2 I_1^3 + \frac{\beta_3 I_1}{2\sqrt{I_2}} \right) \mathbf{B} - \frac{\beta_3}{\sqrt{I_2}} \mathbf{B}^2 + \left[-\frac{2}{3} \left(\beta_1 I_1 + \frac{\beta_3 I_2}{\sqrt{2}} \right) - \frac{8}{3} \beta_2 I_1^3 \right] \mathbf{I}, \tag{16}$$

$$\sigma = \frac{2}{J} \left(\beta_1 + 4\beta_2 I_1^{*3} + \frac{\beta_3 I_1^*}{2\sqrt{I_2^*}} \right) \mathbf{B}^* - \frac{\beta_3}{J\sqrt{I_2^*}} (\mathbf{B}^*)^2 + \left[K(J-1) - \frac{2I_1^*}{3J} (\beta_1 + 4\beta_2 I_1^{*3}) - \frac{2I_2^*}{3J} \left(\frac{\beta_3}{\sqrt{I_2^*}} \right) \right] \mathbf{I}, \tag{17}$$

where the subscript * denotes the deviatoric components.

The Cauchy stress expressions given in Eqs. (16) and (17) are for arbitrary loading response. What differentiates each loading mode is the deformation gradient. The schematic differences between the loading modes and their respective deformation gradients is shown in Fig. 4.

For each of the loading modes, numerical codes that calculate for Cauchy stress (according to Eqs. (16) and (17)) from given vectors of material parameters and the

engineering strains were written and implemented in Python programming language. On the other hand, FE simulation was realized using the commercial FE code Abaqus CAE 2016 as it provides researchers with an opportunity to implement their material models via a user material subroutine. In this case, a vectorized user material (VUMAT) was coded in FORTRAN language and implemented according to the algorithm shown in Fig. 5. It is worth noting that for hyperelastic materials in Abaqus, the stress should be returned in a co-rotational coordinate system in which the basis system rotates with the material. For this reason, the stress must be rotated back before updating the new stresses as shown in

the second last step of the algorithm.

To compare the simulation and the experimental results for uniaxial loading, the workpiece geometry was modeled according to the dimensions of the specimen used by Treloar [19] in his experiments (see Fig. 6a, i). The simulation set-up was simplified by modeling only one-quarter of the workpiece as shown in Fig. 6a, ii and utilizing symmetry boundary conditions. The model was meshed with a total of 6000 full integration 8-node linear brick elements

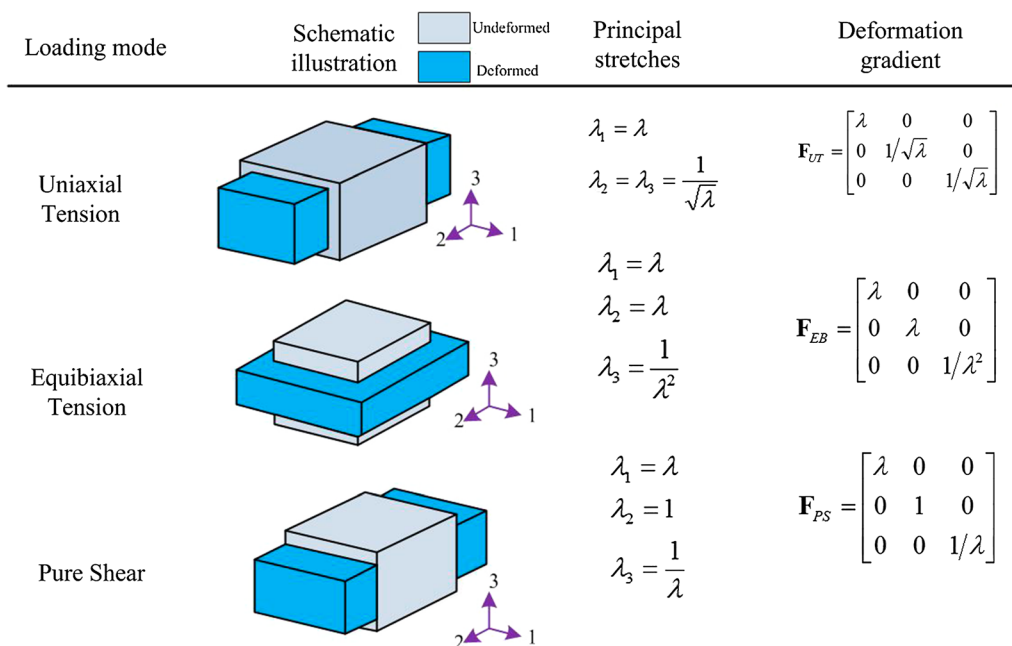


Fig. 4 Schematic illustration of the uniaxial tension, equibiaxial tension, and pure shear loading modes with their respective deformation gradients

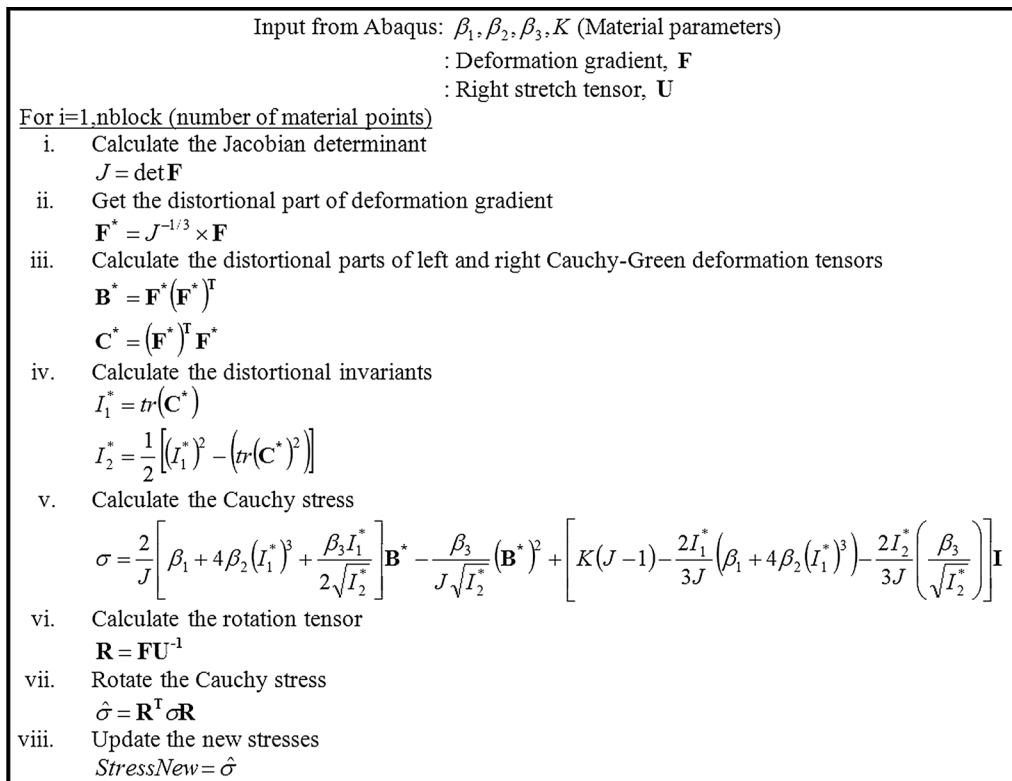


Fig. 5 Algorithm for vectorized user material (VUMAT) implementation in Abaqus CAE

(C3D8) as shown in Fig. 6b. As for the equibiaxial loading, a notched workpiece proposed by Fujikawa et al. [41] in their experiments with geometrical details given in Fig. 6c was used. According to the authors, the notched workpiece helps mitigate the non-uniform deformation between the clamps. The model parameters for the equibiaxial loading ($\beta_1 = 801198.03$, $\beta_2 = 98.58$, $\beta_3 = -527655.25$, $K = 5 \times 10^8$) were obtained by fitting the modified strain energy equation to the strain energy density data calculated from the experimental uniaxial tension data by the authors. For each simulation set-up, a reference point was set to capture both the displacement and force in the direction of the deformation. Since the hyperelastic model is rate-independent, the time taken to complete the simulation doesn't affect the simulation results.

4 Results and discussion

This section presents the numerical predictions of the two models, the original Carroll's and the modified version, compared with Treloar's experimental data for each of the three loading modes namely uniaxial tension, equibiaxial tension, and pure shear. Furthermore, the FE simulation uniaxial tension and equibiaxial tension loading results of the modified Carroll's model are compared with the Treloar's [19] and Fujikawa et al. [41] data of the same loading mode

respectively. The comparison of the models' predictions with the experimental data serves to inform on the predictive abilities of the models. The coefficient of determination, whose expression is given in Eq. (15), is utilized as a measure to indicate how close the model predictions are to the experimental data and hence the accuracy of the model. It is worth noting that to plot engineering stress against the engineering strain, the Cauchy stress from the Python code numerical implementation was converted to engineering stress using the relation $\sigma_{\text{eng}} = \sigma_{\text{true}} / (\epsilon_{\text{eng}} + 1)$.

4.1 Uniaxial tension

Both the original and the modified versions of Carroll's model posted excellent predictions in the uniaxial tension loading with R^2 values of 0.9966 and 0.9986 respectively. That means more than 99% of the predicted data equals the experimental data. As shown in Fig. 7, the classic S-shaped stress-strain curve of this loading mode was reproduced by both models. A closer look at the figure shows that the original Carroll's model is more linear at the beginning of the loading, unlike the modified version which captures the curve hence the small difference between their accuracies. Nevertheless, the difference is negligible and both models can be utilized to accurately predict the behavior of elastomeric materials subjected to uniaxial loading.

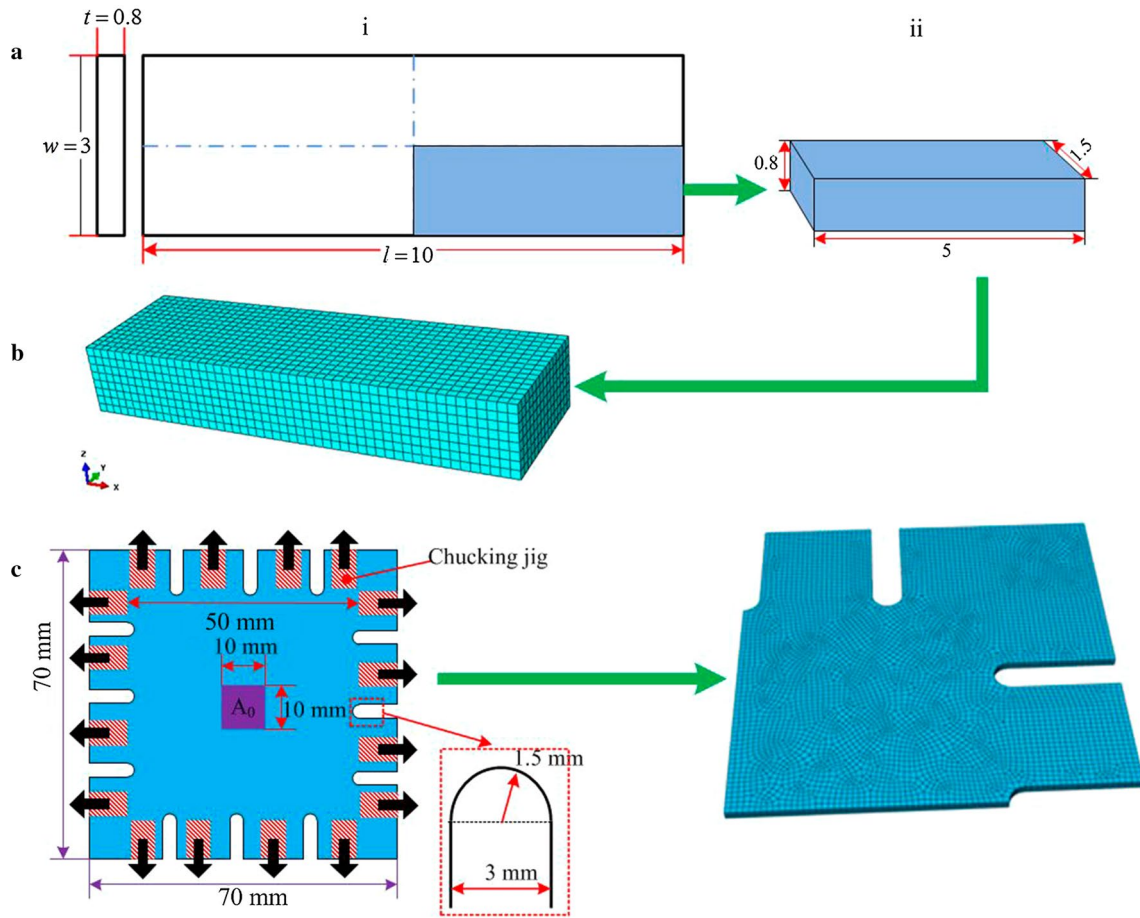


Fig. 6 a, i Geometrical dimensions of the workpiece used by Treloar [19] for uniaxial tension experiments, a,ii details of the one quarter 3D model used in FE simulation, b the meshed 3D model, and c the geometrical details of the workpiece used by Fujikawa et al. [41] for equibiaxial loading and its meshed one quarter 3D model

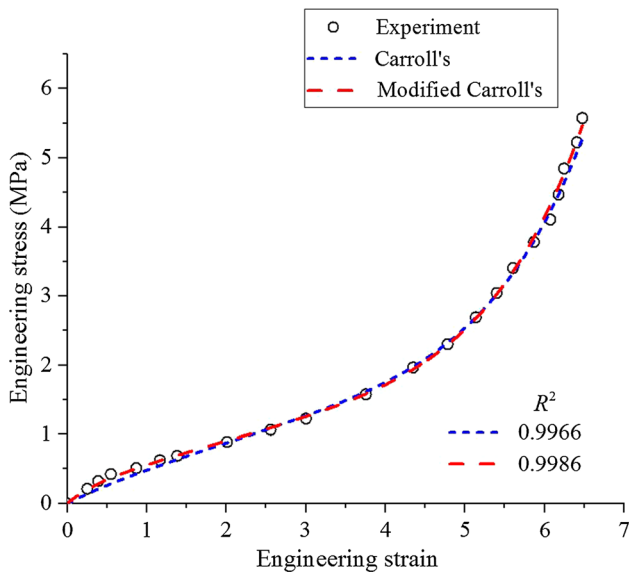


Fig. 7 Comparison of the models' predictions and Treloar's experimental data for uniaxial tension loading

4.2 Equibiaxial tension

This loading mode is crucial for modeling the behavior of elastomeric materials. The challenge with the majority of the hyperelastic models in the literature that require a single pair of model constants for multi-axial loading is that they post accurate predictions in uniaxial and pure shear loading modes but less accurate predictions in equibiaxial loading mode. In this work, the original Carroll's model performs poorly in predicting the equibiaxial tension with R^2 value of -0.4629 as shown in Fig. 8. The negative value simply means that the predictions are below the average horizontal line of the experimental data. On the other hand, the modified Carroll's model posted excellent predictions as indicated by the R^2 value of 0.9843. The second invariant is important for accurate model predictions in equibiaxial tension. From Table 2, it is observed that the third material parameter which is linked with the second invariant in the strain energy density function changes substantially in the modified version as opposed to the

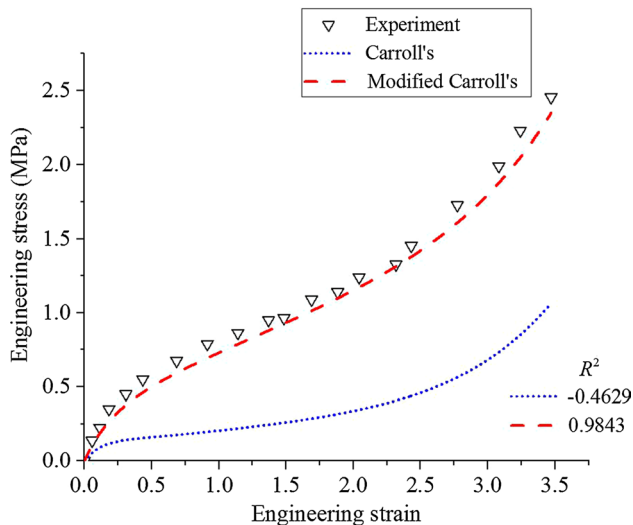


Fig. 8 Comparison of the models' predictions and Treloar's experimental data for equibiaxial tension loading

other two parameters which are relatively comparable. This explains the huge difference in predictions between the two models and also confirms the role of the second invariant in equibiaxial loading.

4.3 Pure shear

Also known as constrained or planar tension test, the specimen is subjected to biaxial tension while being constrained in one direction. As shown in Fig. 9, the modified Carroll's model was able to capture the nonlinear stress–strain behavior observed in experiments with R^2 value of 0.9772. The original Carroll's model is equally good but presents an almost linear stress–strain relationship with R^2 value of 0.9262. In this case, both models can be employed to predict pure shear deformation of elastomers but the modified version is more accurate. It is worth noting that the numerical prediction results for the pure shear and equibiaxial loading as plotted in Figs. 8 and 9 are slightly lower than the experimental data. The difference could be attributed to the material parameters or the strain energy density expression. Simultaneous fitting of the model to the experimental data in all the three modes of loading to obtain model constants could reduce this error. For this work, simultaneous fitting did not yield better results than single fitting using uniaxial tension data.

4.4 FE simulation results

Of interest in the simulation results were the force–displacement data obtained via the reference point in the 3D model

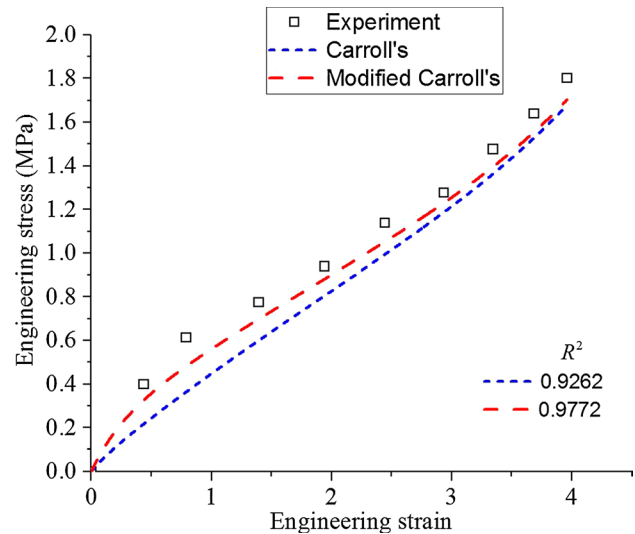


Fig. 9 Comparison of the models' predictions and Treloar's experimental data for pure shear loading

and the stress contour plots at various levels of deformation. Since symmetry boundary conditions were used, the displacement data has to be multiplied by two to get the total displacement. The engineering stress data was obtained by the ratio of the force and the initial cross-sectional area of the 3D model. Similarly, the ratio of the displacement to the original length of the workpiece gave the engineering strain data. A comparison of the simulation and the experimental stress–strain for uniaxial loading is shown by the plots in Fig. 10a, i. The predicted stress distribution at various stages of strain during loading is shown in Fig. 10a, ii. The experimental and simulation stress–strain plots for equibiaxial loading are given in Fig. 10b, i whereas the stress contours at $\epsilon = 0.6$ is shown in Fig. 10b, ii. It can be observed that the simulation predicted the experimentally observed behavior accurately with R^2 value of 0.9465 and 0.9857 for uniaxial tension and equibiaxial tension respectively. This indicates that the VUMAT implementation of the modified Carroll's model was a success and can be reliably used to predict the material's behavior.

5 Conclusions

Carroll's model possesses the desired characteristics of a hyperelastic model such as having few material parameters and that only one set of parameters are required for predicting material response under various types of loading modes. However, its strain energy density function violates one of the most important mathematical restrictions whose physical meaning is that the material should be stress-free at the undeformed state. Moreover, the original version assumed

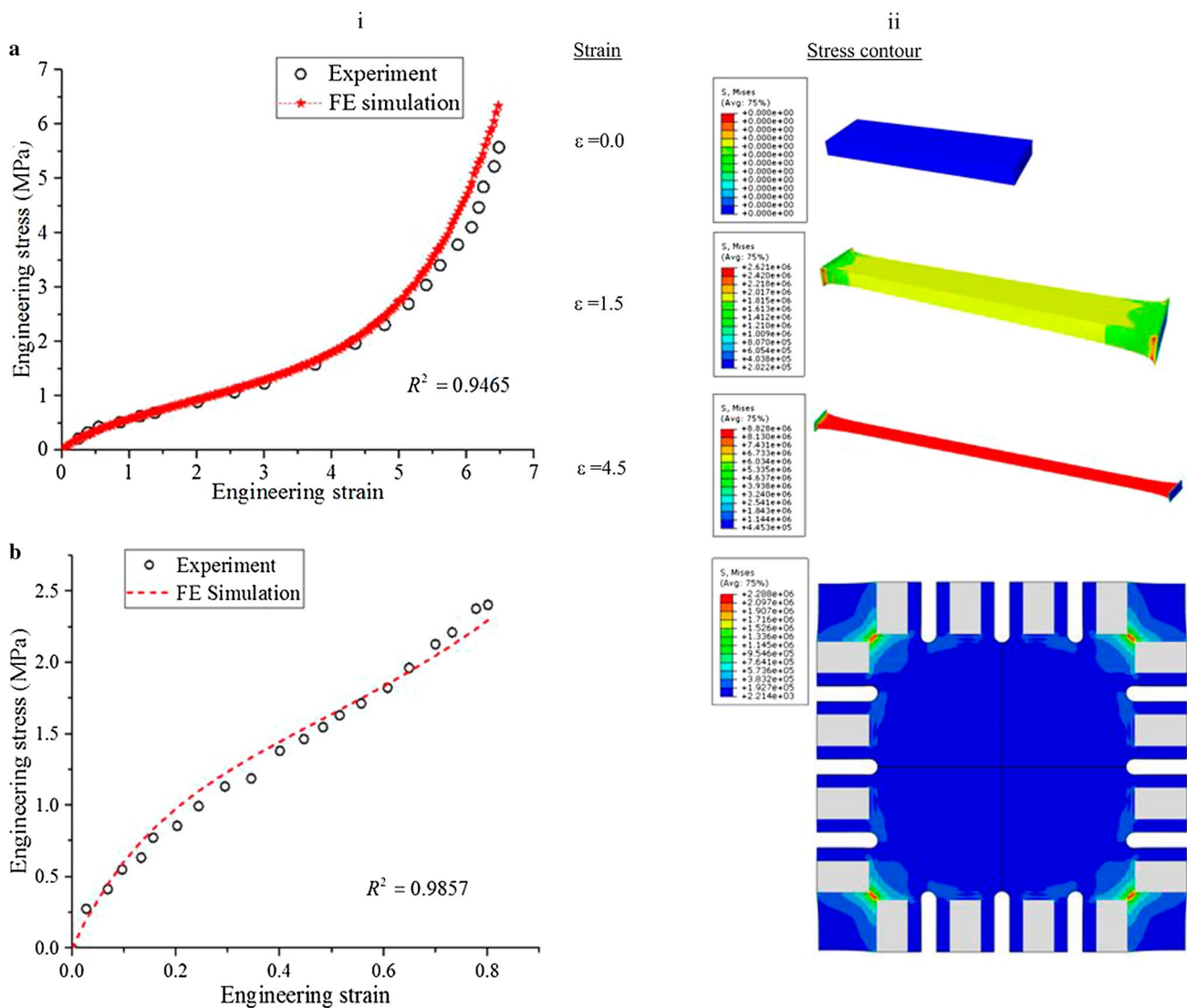


Fig. 10 a,i Comparisons of the modified Carroll's model simulation and the Treloar's [19] experimental stress–strain data for uniaxial tension loading, a,ii stress contours at various stages of loading. b,i Simulation and Fujikawa et al. [41] experimental data for equibiaxial loading, and b,ii the stress contours at $\epsilon = 0.6$ for equibiaxial tension simulation

incompressibility whilst the practical behavior of elastomeric materials includes compressibility and it is important for avoiding numerical problems during finite element implementation.

This work aimed at improving Carroll's model by modifying the strain energy density function according to the mathematical restriction that it should vanish at the undeformed state and by including a compressible term in its expression. According to Treloar's classical experimental data for uniaxial tension loading, the strain energy density was calculated and the Levenberg–Marquardt Algorithm was utilized to fit both the original and the modified strain energy density function to get the material parameters of the model. Cauchy stress equations for arbitrary loading were derived from the strain energy density function and numerical codes

were implemented in Python language to get the model predictions. Furthermore, finite element implementation in Abaqus CAE 2016 via a VUMAT subroutine coded in FORTRAN language was undertaken to demonstrate the capabilities of the modified version in simulating the deformation behavior in uniaxial tension loading.

Comparisons of the model predictions to the classical Treloar's data were presented for each of the loading modes. While the predictions of the original and modified versions were relatively comparable in uniaxial and pure shear loading, the latter outperformed the former in equibiaxial tension loading. The finite element implementation was a great success as the simulation stress–strain results had a good agreement with the corresponding experimental data. This work has demonstrated the superiority of the

modified Carroll's model compared to the original version and its capability to accurately simulate the material response in a finite element implementation.

Acknowledgements The scholarship to the first author by China Scholarship Council is highly appreciated. This work was supported by the National Natural Science Foundation of China (Grants 11632005 and 11672086).

References

- Mooney, M.: A theory of large elastic deformation. *J. Appl. Phys.* **11**(9), 582–592 (1940)
- Chaves, E.W.V.: Hyperelasticity (Chap. 8). In: *Notes on Continuum Mechanics Lecture Notes on Numerical Methods in Engineering and Science*, pp. 423–464. Springer, Dordrecht (2013)
- Hackett, R.M.: Strain-Energy Functions (Chap. 4). In: *Hyperelasticity Primer*, pp. 19–25. Springer, Cham (2016)
- Ruiz, M.J.G., González, L.Y.S.: Comparison of hyperelastic material models in the analysis of fabrics. *Int. J. Cloth. Sci. Technol.* **18**(5), 314–325 (2006)
- Bahreman, M., Darijani, H., Fooladi, M.: Constitutive modeling of isotropic hyperelastic materials using proposed phenomenological models in terms of strain invariants. *Polym. Eng. Sci.* **56**(3), 299–308 (2016)
- Ogden, R.W.: Elasticity (Chap. 4). In: *Non-Linear Elastic Deformations*, pp. 169–229. Dover, New York (1997)
- Arruda, E.M., Boyce, M.C.: A three-dimensional constitutive model for the large stretch behavior of rubber elastic materials. *J. Mech. Phys. Solids* **4**(2), 389–412 (1993)
- Flory, P.J., Erman, B.: Theory of elasticity of polymer networks. 3. *Macromolecules* **15**(3), 800–806 (1982)
- Kaliske, M., Heinrich, G.: An extended tube-model for rubber elasticity: statistical-mechanical theory and finite element implementation. *Rubber Chem. Technol.* **72**(4), 602–632 (1999)
- Treloar, L.R.G.: *The Physics of Rubber Elasticity*, 3rd edn. Oxford University Press, Oxford (1975)
- Yeoh, O.H.: Characterization of elastic properties of carbon-black-filled rubber vulcanizates. *Rubber Chem. Technol.* **63**(5), 792–805 (1990)
- Rivlin, R.S.: Large elastic deformations of isotropic materials. IV. Further developments of the general theory. *Philos. Trans. R. Soc. Lond. A* **241**, 379–397 (1948)
- Horgan, C.O., Saccomandi, G.: Constitutive modelling of rubber-like and biological materials with limiting chain extensibility. *Math. Mech. Solids* **7**(4), 353–371 (2002)
- Beda, T., Chevalier, Y.: Hybrid continuum model for large elastic deformation of rubber. *J. Appl. Phys.* **94**(4), 2701 (2003)
- Boyce, M.C., Arruda, E.M.: Constitutive models of rubber elasticity: a review. *Rubber Chem. Technol.* **73**(3), 504–523 (2000)
- Carroll, M.M.: Molecular chain networks and strain energy functions in rubber elasticity. *Philos. Trans. R. Soc. A* **377**(2144), 20180067 (2019)
- Beda, T.: Modeling hyperelastic behavior of rubber: a novel invariant-based and a review of constitutive models. *J Polym Sci Part B: Polym Phys* **45**(13), 1713–1732 (2007)
- Badienia, Y.: A comparative study of the fitting performance of hyperelastic constitutive models. Middle East Technical University Thesis, 2019
- Treloar, L.R.G.: Stress-strain data for vulcanized rubber under various types of deformation. *Rubber Chem. Technol.* **17**(4), 813–825 (1944)
- Kaoye, L., Bienaimé, M., Blaise, B., Beda, T.: Characterization of hyperelastic deformation behavior of rubber-like materials. *SN Appl. Sci.* **2**, 648 (2020)
- Miroshnychenko, D., Green, W.A.: Heuristic search for a predictive strain-energy function in nonlinear elasticity. *Int. J. Solids Struct.* **46**(2), 271–286 (2009)
- Xintao, Fu., Wang, Z., Ma, L., Zou, Q.Z.Z., Guan, X.: Temperature-dependence of rubber hyperelasticity based on the eight-chain model. *Polymers* **12**(4), 932 (2020)
- Yaya, K., Bechir, H.: A new hyper-elastic model for predicting multi-axial behaviour of rubber-like materials: formulation and computational aspects. *Mech. Time Depend. Mater.* **22**, 167–186 (2018)
- Khajehsaeid, H., Arghavani, J., Naghdabadi, R.: A hyperelastic constitutive model for rubber-like materials. *Eur. J. Mech. A* **38**, 144–151 (2013)
- Zhao, Z., Xihui, Mu., Fengpo, Du.: Modeling and verification of a new hyperelastic model for rubber-like materials. *Math. Probl. Eng.* **2019**, 2832059 (2019)
- Kulchu, I.D.: A hyperelastic constitutive model for rubber-like materials. *Arch. Appl. Mech.* **90**, 615–622 (2020)
- Carroll, M.M.: A strain energy function for vulcanized rubbers. *J. Elast.* **103**, 173–187 (2011)
- Steinmann, P., Hossain, M., Possart, G.: Hyperelastic models for rubber-like materials: consistent tangent operators and suitability for Treloar's data. *Arch. Appl. Mech.* **82**, 1183–1217 (2012)
- Ogden, R.W., Raymond William Ogden: Large deformation isotropic elasticity—on the correlation of theory and experiment for incompressible rubberlike solids. *Proc. R. Soc. Lond. A* **326**(1567), 565–584 (1972)
- Horgan, C.O., Murphy, J.G.: Constitutive modeling for moderate deformations of slightly compressible rubber. *J. Rheol.* **53**(1), 153–168 (2009)
- Reddy, J.N.: *An Introduction to Continuum Mechanics*, 2nd edn. Cambridge University Press, Cambridge (2013)
- Horgan, C.O., Smayda, M.G.: The importance of the second strain invariant in the constitutive modeling of elastomers and soft biomaterials. *Mech. Mater.* **51**, 43–52 (2012)
- Bergström, J.: *Mechanics of Solid Polymers: Theory and Computational Modeling*. Elsevier, Amsterdam (2015)
- Bischoff, J.E., Arruda, E.M., Grosh, K.: A new constitutive model for the compressibility of elastomers at finite deformations. *Rubber Chem. Technol.* **74**(4), 541–559 (2001)
- Horgan, O., Saccomandi, G.: Constitutive models for compressible nonlinearly elastic materials with limiting chain extensibility. *J. Elast.* **77**, 123–138 (2004)
- Yuan, Lu., Zhi-Xiang, Gu., Yin, Z.-N., Xiao, H.: New compressible hyper-elastic models for rubberlike materials. *Acta Mech.* **226**, 4059–4072 (2015)
- Ogden, R.W., Saccomandi, G., Sgura, I.: Fitting hyperelastic models to experimental data. *Comput. Mech.* **34**, 484–502 (2004)
- Levenberg, K.: A method for the solution of certain non-linear problems in least squares. *Q. Appl. Math.* **2**(2), 164–168 (1944)
- Marquardt, D.W.: An algorithm for least-squares estimation of non-linear parameters. *J. Soc. Ind. Appl. Math.* **11**(2), 431–441 (1963)
- Yifeng, Wu., Wang, H., Li, A.: Parameter identification methods for hyperelastic and hyper-viscoelastic models. *Appl. Sci.* **6**(12), 386 (2016)
- Fujikawa, M., Maeda, N., Yamabe, J., Koishi, M.: Performance evaluation of hyperelastic models for carbon-black-filled SBR vulcanizates. *Rubber Chem. Technol.* **93**(1), 142–156 (2020)

Publisher's note Springer Nature remains neutral with regard to jurisdictional claims in published maps and institutional affiliations.